Particle heating and acceleration in regions of magnetic flux emergence

Loukas Vlahos[1]

Department of Physics, Aristotle University,
54124 Thessaloniki, Greece
vlahos@astro.auth.gr

January 8, 2019

Main points

1. The turbulent photosphere drives the active region magnetic field in the state of turbulent reconnection. From turbulence to current sheets and turbulent reconnection. We define as turbulent reconnection the plasma state were large amplitude magnetic fluctuations and Unstable Current Sheets (UCS) co-exist and are responsible for the coronal heating and acceleration of particles in confined flares. (MHD)

2. Emerging magnetic flux interacting with the ambient magnetic field or loss of stability of emerged large scale magnetic structures form large scale current sheets which spontaneously fragment and lead again to turbulent reconnection From large scale current sheets to turbulence. (MHD)

3. How particles are heated and accelerated inside a turbulent reconnecting environment? (MHD+Kinetic)

Spontaneous formation of Reconnecting Current Sheets in the turbulent corona driven by the turbulent photosphere
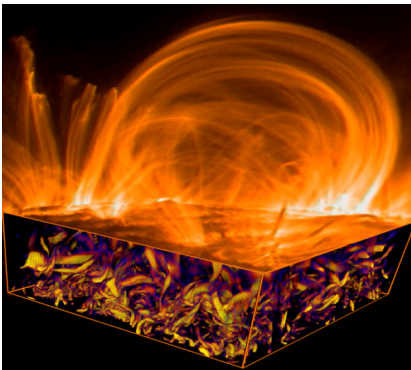
Figure: Stressed from the turbulent convection zone magnetic fields form a turbulent reconnection environment in the Solar Active Regions
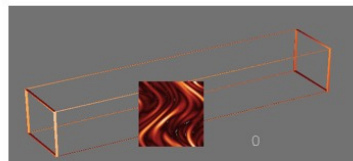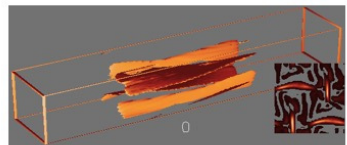
Externally driven turbulent reconnection

Parker was the first to introduce the concept of driven **turbulent reconnection** in the solar corona. [Parker (1983), Parker (1988), Einaudi et al. (1996), Galsgaard and Nordlund (1996), Georgoulis et al. (1998), Rappazzo et al. (2010), Rappazzo et al. (2013), Dahlburg, et al. (2016)]. The random forcing of magnetic field lines at the photosphere develops spontaneously a turbulent reconnection environment in the corona. The initial magnetic topology is usually a single loop or dipole. Two aspects in our numerical experiments are crucial: The the driver and the the initial magnetic topology

Externally driven turbulent reconnection

see details in [Galsgaard and Nordlund (1996)]

The stochastically driven loop model
(Galsgaard)

- 3D MHD experiment of photospherically driven slender magnetic flux tubes

- Continued random driving of the foot points (incompressible sinusoidal large scale shear motions)

- Reconnection jets generate secondary perturbations in B

- Formation of stochastic current sheets

Externally driven turbulent reconnection

Rappazzo et al [Rappazzo et al. (2010)] initiate their simulation with uniform and strong magnetic field tracing the coronal loop between the photospheric planes. At the photosphere a velocity field in the form of a one-dimensional shear flow pattern is present.
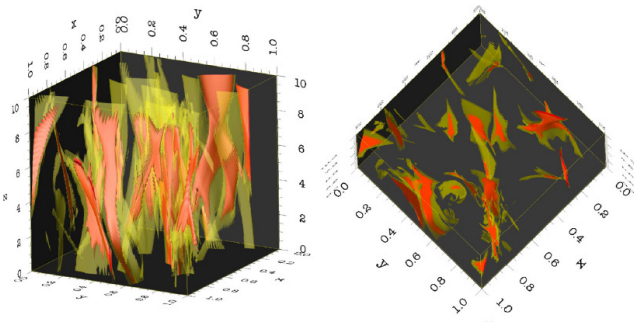

Figure: Isosurfaces corresponding to higher values of j^2. The current sheets filling factor value is small.

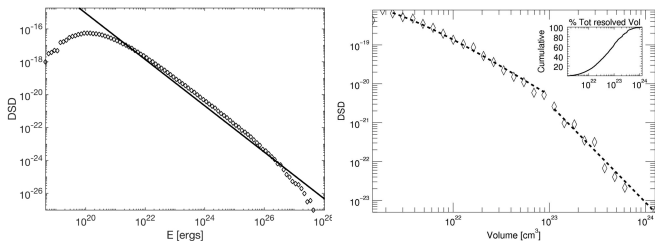# Statistical Properties of Unstable Current Sheets

Kanella and Gudiksen
[Kanella and Gudiksen (2017), Kanella and Gudiksen (2018)]
derive their initial magnetic field from the potential extrapolation
of a magnetic dipole in the photosphere and as driver they use a
continuous random forcing.
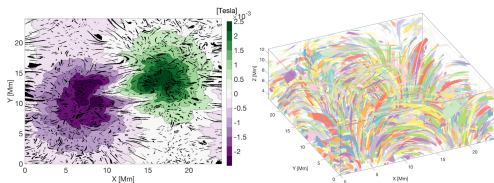
Figure: Left: Contours of the vertical component of the magnetic filed at
the base of the corona (at t=1130sec) together with the bases of the
identified heating events, Right: Identified features of coronal heating.

Statistical Properties of Unstable Current Sheets

Figure: Left: Differential Size Distribution of the identified features' energy rate, the slope is 1.5, Right: DSD of the identified features, volume with slopes 1.53 and 2.53.

Statistical Properties of Unstable Current Sheets

Knizhnik et al [Knizhnik et al. (2018)] use a cylindrical loop, driven by a helical twist $\Omega(r, t) = Ag(r)f(t)$
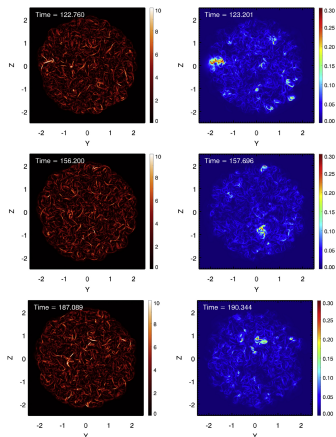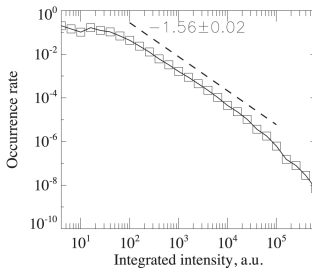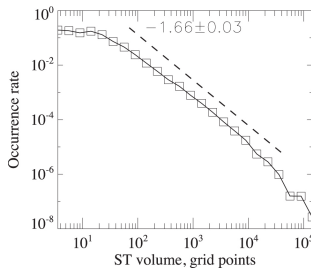
Statistical Properties of Unstable Current Sheets
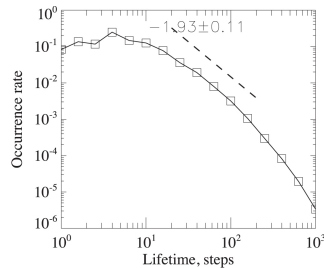
Statistical Properties of Unstable Current Sheets

Statistical analysis of current sheets in three dimensional MHD turbulence

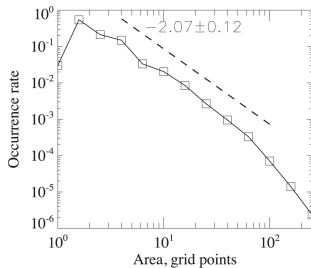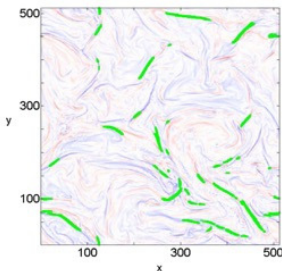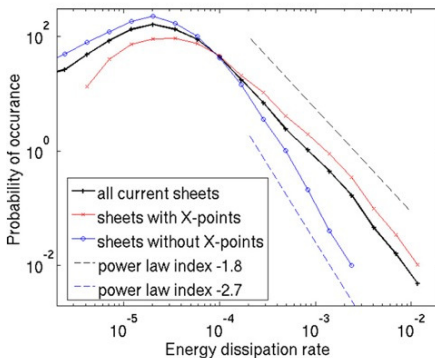Zhdankin et al, ApJ, 2013

Statistical Properties of Unstable Current Sheets

[Zhdankin et al. (2013)]

Energy dissipation rate

Summary of my first point

Level 1: From turbulence to turbulent reconnection

The photospheric turbulence spontaneously initiate large amplitude magnetic fluctuations and Unstable Current Sheets (UCS) with a relatively small filing factor in the magnetic topology. The UCS interact with their jets or evolve and enhance the ambient turbulence in the corona [Galsgaard and Nordlund (1996), Pucci et al. (2018), Karimabadi et al. (2014)]. The statistical properties of the UCSs are almost universal when the Active Regions reach the state of turbulent reconnection. Coronal heating and confined flares are the result of these physical processes. More on how particles react on such strongly turbulent environment are published in a series of articles published recently [Vlahos et al. (2016), Pisokas et al. (2018), Li et al. (2018), Zhdankin et al. (2018), Comisso and Sironi (2018)]).

Formation of strong turbulence environment from magnetic flux emergence and jet formation
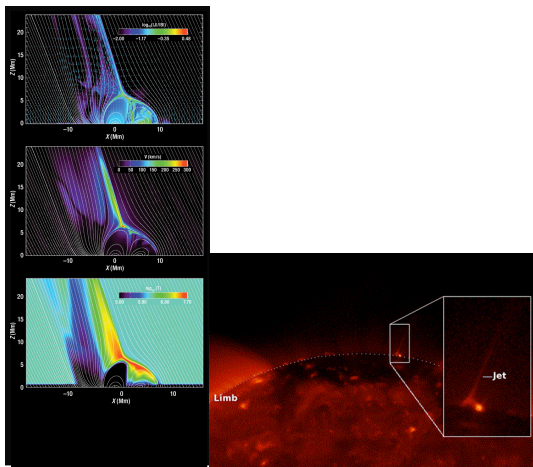
Formation of strong turbulence environment during explosive events on the Sun

The MHD simulations presented here were based on the article of Archontis and Hood (2013) [Archontis and Hood (2013)] and will we plan to submit soon an article on "Particle acceleration and heating in regions of magnetic flux emergence" by Isliker, Archontis and Vlahos.
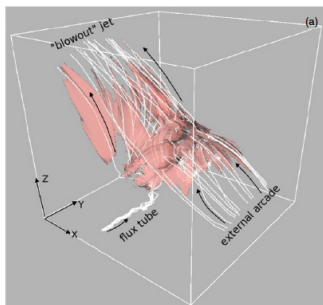
Formation of large scale current sheets and their fragmentation

The evolution of a forced reconnection undergoes two major steps : Formation of the standard jet at tilmestep 30, and blow out jet around the time step 53.
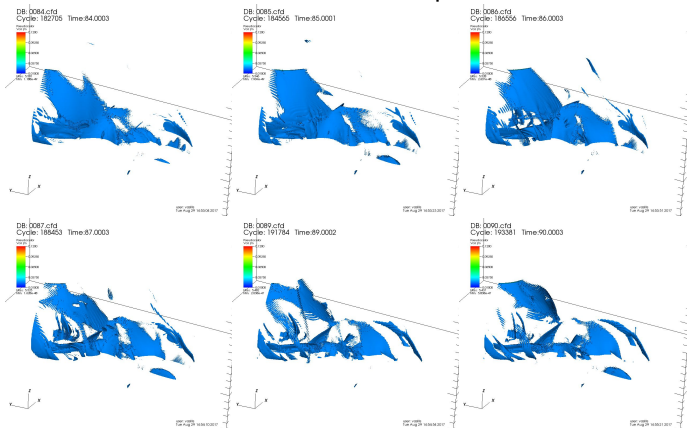
Formation of strong turbulence environment from the fragmentation of large scale current sheet
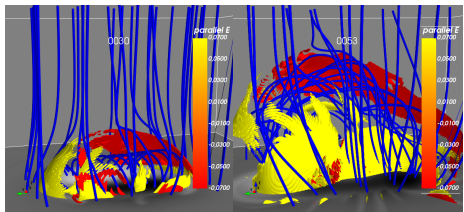
Figure: MHD simulations, in the left the snapshot 30, zoom into the coronal part: Magnetic field lines (blue tubes), together with an iso-contour plot of the electric field (red to yellow 3D-surfaces). At the bottom x-y-plane, the photo-spheric component B_z is shown as a 2D filled contour plot. The parallel electric field is in physical units [V/m]. Right: MHD simulations, snapshot 53, zoom into the coronal part: Magnetic field lines (blue tubes), together with an iso-contour plot of the parallel electric field (red to yellow 3D-surfaces, for the thresholds

Statistical analysis of the parallel electric filed
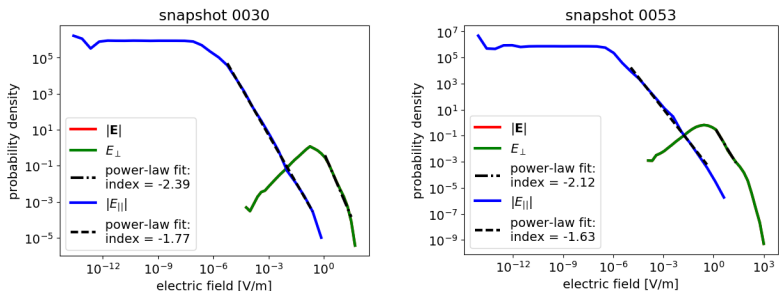
Figure: MHD simulations, snapshot 30 and 53, coronal part only: Distribution of the magnitude of the electric field from all coronal grid-points, for the total electric field, the perpendicular component (they practically coincide), and the parallel component, respectively. The electric field is in units [V/m], and the mean Dreicer field is 4.6×10^{-4} V/m.

Fractal distribution of the fragmented current sheets
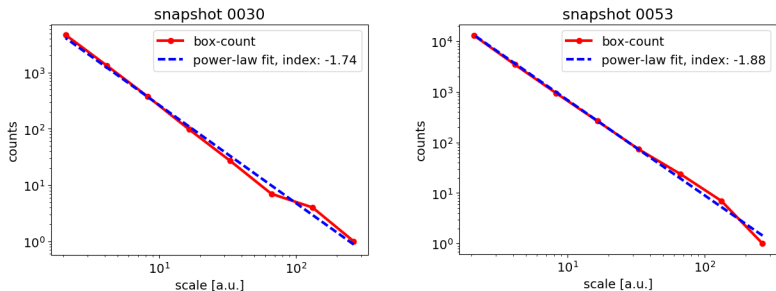
Figure: Scaling of the 3D box-counting algorithm, for snapshot 30 and 53.

Summary of Point Two

From large scale current sheets to turbulent reconnection

We claim that the statistical properties of the fragmented large scale current sheet, formed on the interface of emerging magnetic rope and the ambient open field, can reach universal power laws in the electric field, have fractal spatial distribution around 2. The last point mean that the fragments are concentrated along a 2D surface in this particular numerical experiment. Unfortunately, very few MHD studies have analyzed the statistical properties of the current fragmentation in well developed strongly turbulent plasmas so far.

Summary of Point Two

From large scale current sheets to turbulent reconnection

The key differences from the results reported on the turbulence driven reconnection reported earlier are: (1) the fragmentation of the large scale current sheets creates an environment with higher filing factor and (2) the impulsive initiation of the fragmentation of the large scale current sheet. Both these factors help the explosive events to become more efficient on particle heating and acceleration. I have left out from my discussion here the other large scale non linear structure naturally formed in the explosive events, which is the shock. My opinion is that this too will lead to turbulent reconnection [Karimabadi et al. (2014)] .

Level 3 (MHD+kinetic): Test particle evolution inside the MHD fields

The relativistic guiding center equations (without collisions) are used for the evolution of the position $\mathbf{r}$ and the parallel component $u_{\|}$ of the relativistic 4-velocity of the particles,

$$\frac{d\mathbf{r}}{dt} = \frac{1}{B_{\|}^*}\left[\frac{u_{\|}}{\gamma}\mathbf{B}^* + \hat{\mathbf{b}} \times \left(\frac{\mu}{q\gamma}\nabla B - \mathbf{E}^*\right)\right] \qquad (1)$$

$$\frac{du_{\|}}{dt} = -\frac{q}{m_0 B_{\|}^*}\mathbf{B}^* \cdot \left(\frac{\mu}{q\gamma}\nabla B - \mathbf{E}^*\right) \qquad (2)$$

where $\mathbf{B}^* = \mathbf{B} + \frac{m_0}{q}u_{\|}\nabla \times \hat{\mathbf{b}}$, $\mathbf{E}^* = \mathbf{E} - \frac{m_0}{q}u_{\|}\frac{\partial \hat{\mathbf{b}}}{\partial t}$, $\mu = \frac{m_0 u_{\perp}^2}{2B}$ is the magnetic moment, $\gamma = \sqrt{1 + \frac{u^2}{c^2}}$, $B = |\mathbf{B}|$, $\hat{\mathbf{b}} = \mathbf{B}/B$, $u_{\perp}$ is the perpendicular component of the relativistic 4-velocity, and q, m_0 are the particle charge and rest-mass, respectively.

Initiating the particles
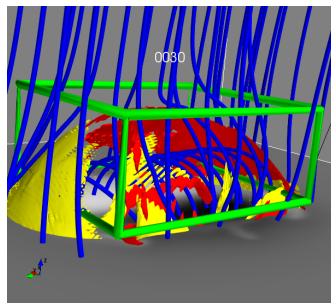
Figure: MHD simulations, snapshot 30, zoom into the coronal part: Magnetic field lines (blue tubes), together with an iso-contour plot of the parallel electric field (red to yellow 3D-surfaces), for the 2 thresholds discussed earlier the photo-spheric component B_z is shown as a 2D filled contour plot. The region in which the spatial initial conditions are chosen is out-lined by a green cube.

Particle energy distributions
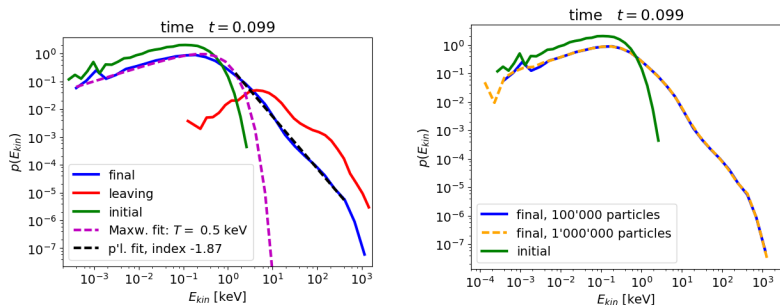
Figure: Snapshot 30: Kinetic energy distribution of electrons after $\approx 0.1\,\mathrm{s}$ (top left), without collisions, together with a fit at the low-energy, Maxwellian part and the high energy, power-law part, the initial distribution, and the distribution of the leaving particles (for every particle at the time it leaves). Top right: Comparison of the kinetic energy distributions from simulations with 100'000 and 1'000'000 test-particles, respectively.

Particle energy distributions
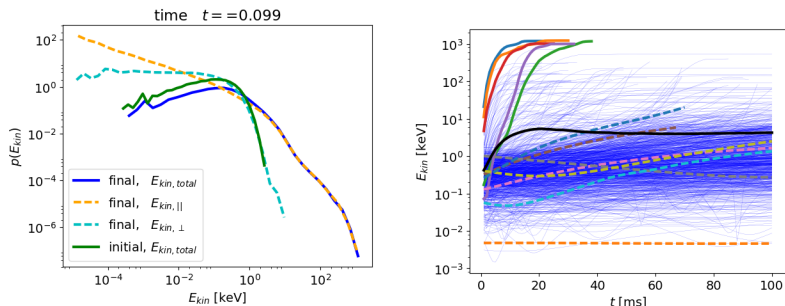
Figure: Snapshot 30: ≈ 0.1 s left: comparison of the total kinetic energy, the parallel, and the perpendicular kinetic energy at 0.1s. right: Kinetic energy of particles as a function of time (thin blue lines), with a few trajectories marked with bold lines (solid at high energies and dashed at low energies), together with the mean energy (solid black).

Heating
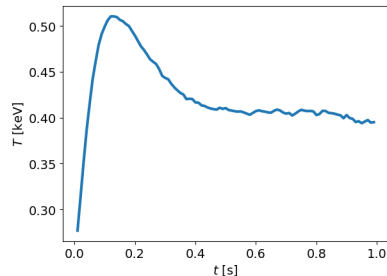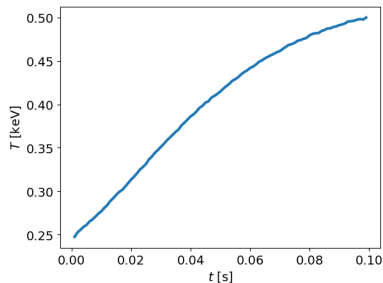
Figure: Snapshot 30: Temperature as a function of time, as determined through the fit of a Maxwellian in the low energy range of the kinetic energy distribution.

Evolution of the distribution for "short" and "long" times
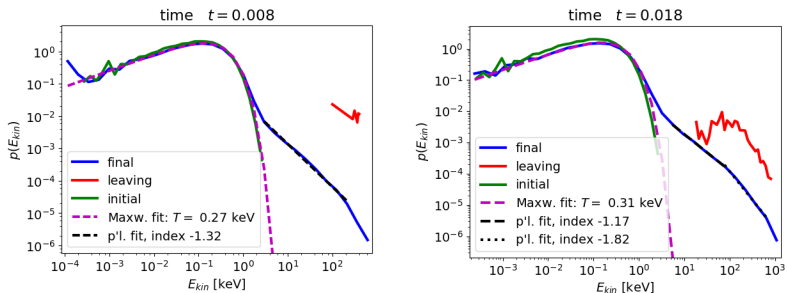
Figure: Snapshot 30: Kinetic energy distribution of electrons after $\approx 0.01\,\text{s}$ (left), $\approx 0.02\,\text{s}$ (right), $\approx 0.1\,\text{s}$

Evolution of the distribution for "short" and "long" times
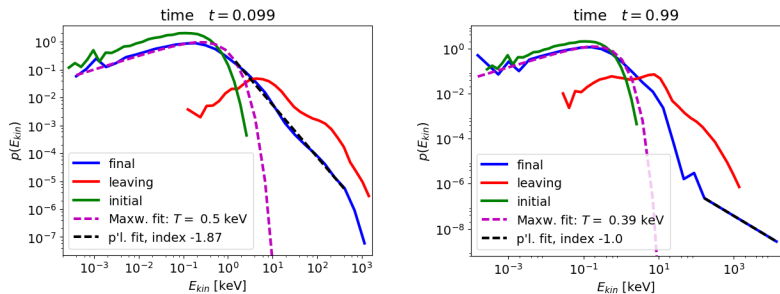
Figure: Snapshot 30: (left) and ≈ 1.0 s (right), without collisions, together with a fit at the low-energy, Maxwellian part and the high energy, power-law part, the initial distribution, and the distribution of the leaving particles (for every particle at the time it leaves).

The role of collisions
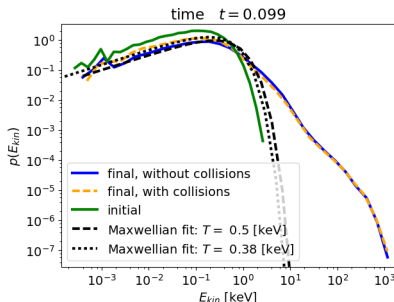
Figure: Snapshot 30: Kinetic energy distribution of electrons after 0.1 sec, without collisions (blue) and with collisions (orange), together with the initial distribution (green).

The blowout jet
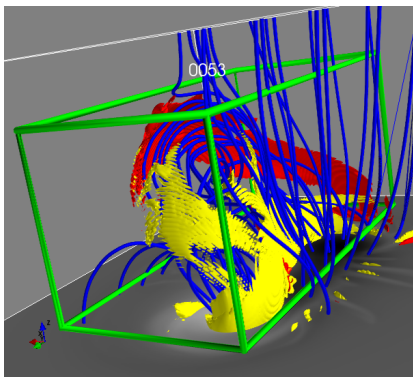
Figure: MHD simulations, snapshot 53, zoom into the coronal part: Magnetic field lines (blue tubes), together with an iso-contour plot of the parallel electric field (red to yellow 3D-surfaces), for the 2 thresholds discussed above. The green cube outlines the region from which the initial conditions are chosen.

Particle dynamics in the blowout jet
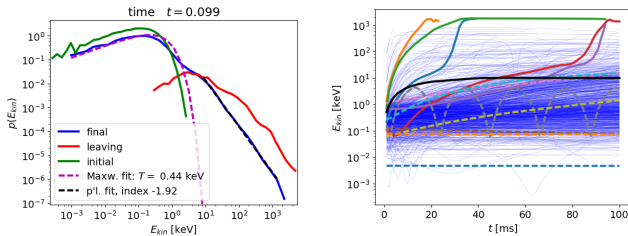
Figure: Snapshot 53: Kinetic energy distribution of electrons after 0.1 sec, without collisions, together with a fit at the low-energy, Maxwellian part and the high energy, power-law part, the initial distribution, and the distribution of the leaving particles (for every particle at the time it leaves) (left). Kinetic energy as a function of time for the test-particles (thin lines), with a few high energy (solid) and low energy (dashed) particles marked with colors, together with the evolution of the mean value (solid black).

Observations

Several RHESSI observations from the base of coronal jets are associated with Hard-X Ray (HXR) emission [Bain and Fletcher (2009), Glesener et al. (2012)]. Frequently during coronal jets the temporal profile of the associated HXRs matches the associated type III radio bursts [Chen et al. (2013)]. Impulsive solar energetic particle events are also related with the jets (see review by [Raouafi et al. (2016)]). It is then obvious that jets act as an efficient mechanism for the heating and acceleration of particles, mainly due to the reconnecting current sheets in the boundary between the emerging magnetic flux and the ambient magnetic field in the solar atmosphere.

Transport in fragmented current sheets: Energy transport

How we will estimate the transport coefficients using the wealth of data collected from the orbits analysed above?

A first and classical candidate for a statistical transport model is the Fokker-Planck equation, which in energy space writes as

$$\frac{\partial f}{\partial t} = \frac{\partial}{\partial E}\left[\frac{\partial(Df)}{\partial E} - Ff\right] - \frac{f}{\tau_{esc}} \tag{3}$$

with D the diffusion and F the convection coefficient, and τ_{esc} the escape time. In this approach, the basic step is the determination of the two transport coefficients, D and F, which we derive here from the test-particle simulation data.

Energy transport

An estimate of the energy-dependence of the transport coefficients, for a given time t_k, is made by first prescribing bins along the E_{kin}-axis, with mid-points E_i ($i = 1, ..., n$), and then considering $E_{kin,j}(t_{k+h}) - E_{kin,j}(t_k)$ a function of E_i if $E_{kin,j}(t_k)$ lies in the bin i. The functional form of the transport coefficients, defined as

$$D\left(t_k, E_i\right) = \frac{1}{2(t_{k+h} - t_k)} \left\langle \left(E_{kin,j}(t_{k+h}) - E_{kin,j}(t_k)\right)^2 \right\rangle_j (t_k, E_i)$$
(4)

and

$$F\left(t_k, E_i\right) = \frac{1}{(t_{k+h} - t_k)} \left\langle E_{kin,j}(t_{k+h}) - E_{kin,j}(t_k) \right\rangle_j (t_k, E_i)$$
(5)

can then be determined by applying binned statistics, i.e. by calculating the mean values for each bin separately at a given time instance t_k.

Energy transport
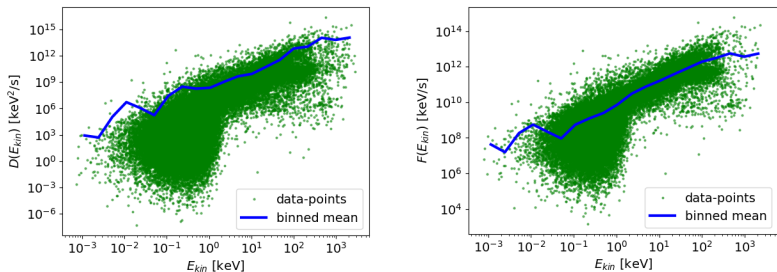
Figure: Snapshot 53: Diffusion coefficient D (left), and convective coefficient F (right), as a function of the kinetic energy, at time $t \approx 0.1\,\text{s}$, together with the data-points on which the binned statistics is based.

Energy transport

The diffusion and drift coefficient for snapshot 53 at $t = t_{100} \approx 0.1\,\mathrm{s}$, together with the data-points that form the sample of the binned statistics ($\epsilon_j(t_{100})^2$ and $\epsilon_j(t_{100})$, respectively, as a function of $E_{kin,j}(t_{100})$). The binned mean for both coefficients exhibits quite a clear power-law functional form, yet the spread of the data points around the mean values is large, namely several orders of magnitude, which is a first hint that the estimate of the transport coefficients is problematic.

Is the Fokker-Planck equation a valid approximation for particle acceleration in strongly turbulent plasmas?
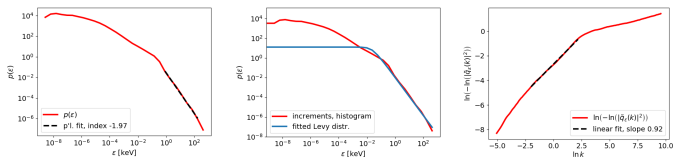
Figure: Snapshot 53, $t \approx 0.1\,\mathrm{s}$: (a) Distribution of energy increments. (b) One-sided distribution of energy increments, together with fitted stable Levy distribution. (d) Characteristic function estimate.

Is the Fokker-Planck equation a valid approximation for particle acceleration in strongly turbulent plasmas?

We show in the previous slides that the histogram $p(\epsilon)$ of the energy increments ϵ_j, which follows a double power-law distribution, with index -1.97 at the highest energies. It then follows that the drift coefficient F, as a mean values of the increments, is not representative for the scale-free data, and the diffusion coefficient D, as a variance of the increments, is ill-defined. This result, namely that the Fokker-Planck formalism breaks down, has been found also for the cases of strong turbulence [Isliker et al. (2017)] and of turbulent reconnection [Isliker et al. (2017)].

Is the Fokker-Planck equation a valid approximation for particle acceleration in strongly turbulent plasmas?

The power-law tail of the distribution of energy increments implies that the particle dynamics is anomalous, with occasionally large energy steps being made, the particles perform Levy-flights in energy space. In [Isliker et al. (2017)], we have introduced a formalism for a fractional transport equation (FTE) that is able to cope with this kind of non-classical dynamics.

Fractional Transport Equation

The FTE has the form [Isliker et al. (2017)]

$$\frac{\partial f}{\partial t} = \frac{a}{\Delta} D^{\alpha}_{|E|} f - \frac{f}{\tau_{esc}} \qquad (6)$$

with $D^{\alpha}_{|E|}$ the symmetric Riesz fractional derivative of order α (defined in Fourier space as $\mathcal{F}(D^{\alpha}_{|E|} f) = -|k|^{\alpha} \hat{f}$), a the constant of the Levy stable distribution that is related to the width of the distribution of increments, and Δ the applied time-step in monitoring the particles' energies.

Solution of the Fractional Transport Equation
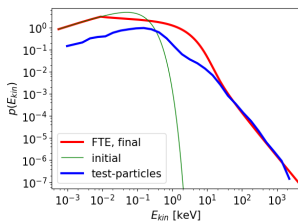
Figure: Snapshot 53: Kinetic energy distribution at initial ($t \approx 0.1\,\mathrm{s}$) and final time, together with solution of the FTE at final time.

Spatial Diffusion

We define the spatial mean square displacement (MSD) as

$$\left\langle \rho_j^2 \right\rangle := \frac{1}{2(t_{k+h} - t_k)} \left\langle (\mathbf{x}_j(t_{k+h}) - \mathbf{x}_j(t_k))^2 \right\rangle_j \qquad (7)$$

Spatial Diffusion
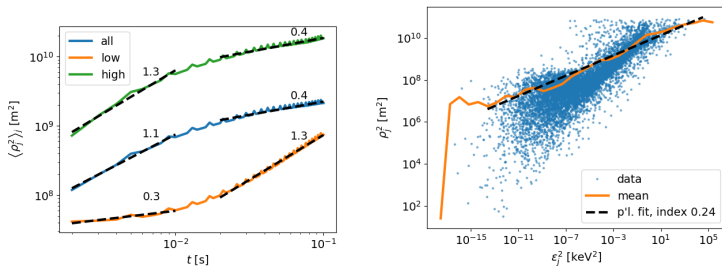
Figure: (a) Instantaneous mean square displacement in space as a function of time for all the particles ('all'), the high ('high') and low ('low') energy particles, together with power law fits (dashed lines), with the numbers indicating the power-law indexes of the fits. (b) Scatter plot of the squared spatial increments ρ_j^2 as a function of the squared energy increments ϵ_j^2, together with the binned mean and a power-law fit to the latter.

Summary of point three

Test particle dynamics is useful tool for analysing the particle heating and acceleration in Strongly Turbulent plasmas

- The statistical properties of the electric fields in the fragments of the current sheets and the overall topology play a crucial role for the heating and acceleration of particles.

- The transport of the particles in space and energy do not obey the Fokker-Planck equation, since their interaction with the strong turbulent fields is anomalous. Particles execute Levy flights in space and energy.

- The need for a Fractional Transport Equations is obvious from our analysis of the particle dynamics inside the strongly turbulent emvironment.

Summary and Discussion

I have stressed the following points:

> **Convection zone and solar eruptions are the drivers for turbulent reconnections in the solar atmosphere**
>
> The magnetic field in the solar corona is always under stress from the driver (convection zone) and gradually or explosively the solar corona is always in a turbulent reconnection state. The characteristics of turbulent reconnection depend on the topology of the complex magnetic field and the properties of the driver.
> Explosive phenomena add complexity to the coronal magnetic field. Current fragmentation and turbulent reconnection are channeled along the large scale topologies (this point sustains the myth of the "standard flare models"). Particles may get their main energisation along the fragments of the main current sheet but they are possibly re-accelerated along their way to the chromoshere or the solar wind by other places undergoing turbulent reconnection along their path.

Summary and Discussion

Heating and acceleration during turbulent reconnection

Heating and particle acceleration naturally sets in, in this open large scale strong turbulent environment. The heating and the acceleration of particles during turbulent reconnection is closely related with the statistical properties of the fragmented currents and the large amplitude magnetic disturbances. One important finding from the analysis of particle dynamics during turbulent reconnection is that the transport properties of high energy particles (systematic acceleration) don't follow the Fokker-Planck equation. The need for a Fractional Transport Equation is apparent from our test particle simulation results.

References I

📄 V. Archontis and A. Hood,
The Astrophysical Journal Letter, 769, L21 (2013).

📄 H.M. Bain and L. Fletcher,
Astronomy and Astrophysics, 508, 1443 (2009).

📄 P. Cargill, L. Vlahos, G. Baumann, J. Drake and A. Nordlund,
Space Science Reviews 173, 223 (2012).

📄 N. Chen, W.H-., Ip and D. Innes,
The Astrophysical Journal 769, 96 (2013).

📄 L. Comisso, and L. Sironi,
arXiv e-print, arXiv:1809.01168 (2018).

References II

📄 R. B. Dahlburg, G. Einaudi, B.D. Taylor, I. Ugarte-Urra, H.P. Warner, A.F. Rappazzo, and M. Velli,
The Astrophysical Journal, 817, 47 (2016).

📄 G. Einaudi, M. Velli, H. Politano, and A. Pouquet,
The Astrophysical Journal Letters, 457, 113 (1996).

📄 K. Galsgaard and A. Nordlund
Journal of Geophysical Research, 101, 13445 (1996).

📄 M. K. Georgoulis, M. Velli and G. Eunaudi,
The Astrophysical Journal, 497, 957 (1998).

📄 L. Glesener, S. Krucker, and R.P. Lin,
The Astrophysical Journal, 754, 9 (2012).

References III

📄 H. Isliker, L. Vlahos and D. Constantinescu,
Physical Review Letters, 119, 045101 (2017).

📄 H. Isliker, Th. Pisokas, L. Vlahos and A. Anastasiadis,
The Astrophysical Journal, 849, 35 (2017).

📄 C. Kanella and V. Gudiksen,
AStronomy and Astrophysics, 603, A83 (2017).

📄 C. Kanella and V. Gudiksen,
Astronomy and Astrophysics, 617, A50 (2018).

📄 H. Karimabadi et al.,
Physics of Plasmas, 21, 062308 (2014).

References IV

📄 K. J. Knizhnik, V.M. Uritsky, J.A. Klimchuk, and C.R. DeVore,
The Astrophysical Journal, 853, 82 (2018).

📄 X. Li, F. Guo, H. Li and S. Li,
The Astrophysical Journal, 866, 4 (2018).

📄 E.N. Parker
The Astrophysical Journal, 264, 642 (1983).

📄 E.N. Parker
The Astrophysical Journal, 330, 474 (1988).

📄 F. Pucci, W.H. Mattheus, A. Chassapis, S. Servido, L. Sorrio-Valvo and G. Lapenta,
The Astrophysical Journal, 867, 10 (2018).

References V

📄 P. Pisokas, H. Isliker and L. Vlahos,
The Astrophysical Journal, 852, 64 (2018).

📄 A. F. Rappazzo, M. Velli, and G. Einaudi,
The Astrophysical Journal, 722, 65 (2010).

📄 A. F. Rappazzo, M. Velli, and G. Einaudi,
The Astrophysical Journal, 771, 76 (2013).

📄 N. E. Raouafi et al.
Space Science Review, 201, 1 (2016).

📄 L. Vlahos, Th. Pisokas, H. Isliker, V. Tsiolis and A. Anastasiadis
The Astrophysical Journal Letters, 827, 3 (2016).

References VI

📄 V. Zhdankin, D. A. Uzdensky, J. C. Perez and S. Boldyrev
The Astrophysical Journal, 771, 124 (2013).

📄 V. Zhdankin, D. A. Uzdensky, G. R. Warner and M.C.J. Begelmsan,
ArXiv e-prints, arXiv: 1809.01966 (2018).